Improving mass-wasting inventories by incorporating debris flow topographic signatures

N. J. Lyons, H. Mitasova & K. W. Wegmann

Landslides
Journal of the International Consortium on Landslides

ISSN 1612-510X

Landslides
DOI 10.1007/s10346-013-0398-0

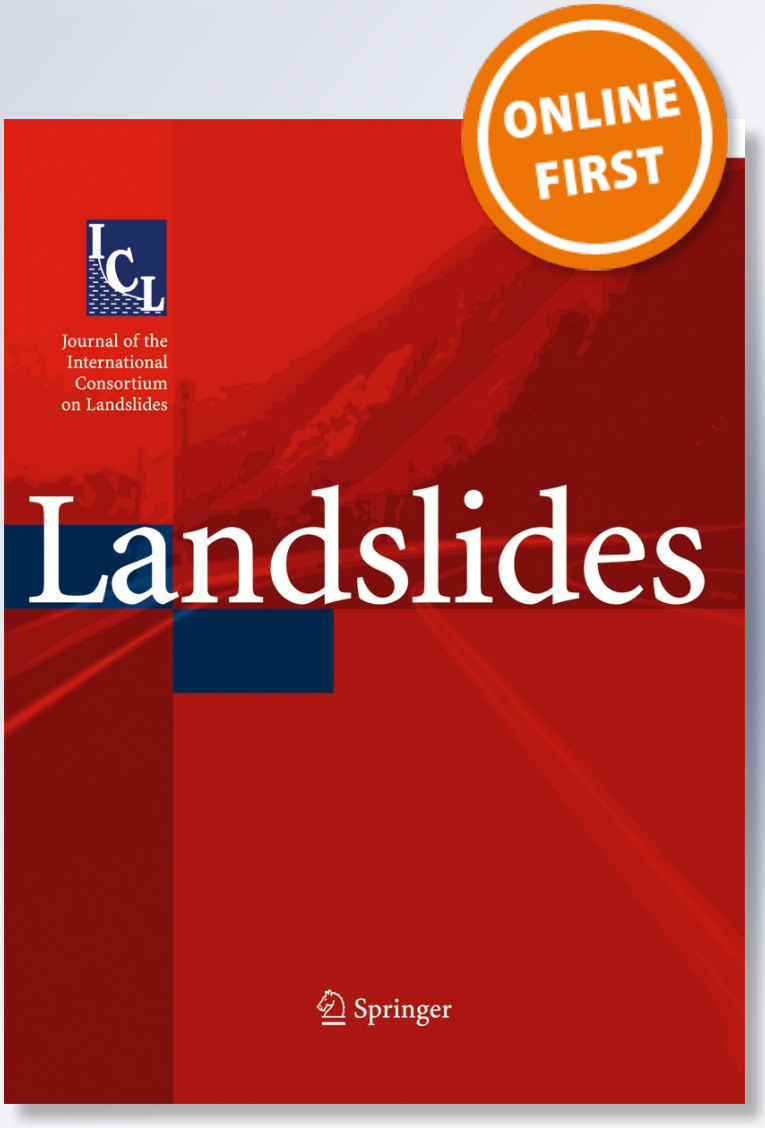

Springer

Original Paper

Landslides
DOI 10.1007/s10346-013-0398-0
Received: 26 July 2012
Accepted: 12 March 2013

N. J. Lyons · H. Mitasova · K. W. Wegmann

Improving mass-wasting inventories by incorporating debris flow topographic signatures

Abstract Debris flows are a prevalent and destructive mass-wasting type in many mountainous regions throughout the world, yet the recent identification of a debris flow topographic signature has not been incorporated into landslide inventories. We have detected this signature in a digital elevation model of the mountainous Oconaluftee River basin of the southern Appalachians, USA, where we have conducted mass-wasting inventories. We evaluate the applicability of this topographic signature in debris flow mapping efforts using inventories created by semiautomated classification of topographic derivative and vegetation index maps. Debris flow detection was increased by 12% when the inventory was limited to the portion of the landscape that exhibits the debris flow topographic signature. The extent of drainages with this topographic signature, which have areas of 6 to 35km^2, is corroborated by analyses of channel form, knickpoint and bedrock distributions, and hypsometry. This mass-wasting inventory technique provides a more focused approach to statistically characterize the land surface, which resulted in increased inventory proficiency across a landscape with an extensive and relatively well-documented debris flow history.

Keywords Landslide · Southern Appalachians · Disaster management · Supervised classification · Landscape evolution · Knickpoint

Introduction

Debris flows can be the primary agent of stream incision, exceeding the efficiency of exclusively fluvial incision processes in valleys with steep slopes and moderate-sized drainages (Hovius et al. 1998; Stock and Dietrich 2003). Debris flows, following the widely used classification system of Cruden and Varnes (1996), are a shallow type of gravitationally-driven mass-wasting, composed of water, rock, soil, and vegetation and triggered by intense and/or frequent precipitation. The hillslope fails on a plane between regolith and bedrock or between heterogeneous layers of soil (Southworth et al. 2005). The mass then flow downslope for distances of up to several kilometers in locations where the hillside slope, channel length, and junction angles permit rapid transportation (Cruden and Varnes 1996). This process can leave a distinct signature in the longitudinal profile of stream channels that indicates the extent of debris flow activity and may reflect phases in the topographic evolution of the landscape (e.g., Howard 1994; Tucker and Slingerland 1997; Pazzaglia et al. 1998; Crosby and Whipple 2006).

Mass-wasting inventories are an important component of hazard modeling (Brardinoni et al. 2003; Malamud et al. 2004; Carrara and Pike 2008). Slope instability models, such as the widely used Shallow Landsliding Stability Model (Dietrich at al. 1992) and Stability Index Mapping (Pack et al. 1998), use inventories to evaluate model results or calibrate parameters (e.g.,Wooten et al. 2008). The model products are used to guide land-use planning to reduce and mitigate the disastrous impacts of future mass-wasting events on the built environment. Unlike the models, the goal of an inventory is to delineate and/or characterize mass-wasting occurrences in a given area. Mass-wasting inventories have also been used in analyses of landscape evolution (Stock and Dietrich 2003; Korup et al. 2010; Gallen et al. 2011). However, relating topographic forms to landscape evolution processes such as debris flows is rarely carried out during a mass-wasting inventory. This paper presents a mass-wasting inventorying technique that is applied to drainages that have the topographic signature of debris flows.

Many published mass-wasting inventories commonly involve the following steps: (1) an area with a history of mass-wasting activity is selected, (2) a technique for identifying and delineating mass-wasting is applied to the area, (3) known false positives, such as roads, are removed, and (4) the performance of the inventory is evaluated against other verification techniques, such as field-based corroboration (e.g., Wegmann 2006). In Step 2, homogeneous land segments are classified into mass-wasting and non-mass-wasting classes by locating areas with the hypothesized or empirically determined properties of the two classes. Class properties are based upon the statistical characterization of topographic, spectral, and/or contextual datasets contained within land segments.

We hypothesize that demarcating inventory areas arbitrarily, such as by catchment or political boundaries, results in non-optimal statistical characterization of the two classes. A more focused characterization may be achieved by limiting the inventory to only areas with the topographic signature of debris flows. We utilize a southern Appalachian field site to test a technique that limits mass-wasting inventories to areas that have the topographic signature of debris flows, which are the most prevalent and destructive mass-wasting type in the region (Witt 2005; Wooten et al. 2008). Furthermore, 92 % of the study location has been managed as part of the Great Smoky Mountains National Park since 1932. Limited human activity, a well understood geologic history, and a region dominated by debris flow mass-wasting are the prerequisites to test this inventory technique.

Background of mass-wasting inventory methods

Until recently, interpretation of aerial photographs has been the standard method to create inventories. New techniques that are quantitative, more robust, and less subjective than air photo interpretation are now made possible by the increased availability of digital elevation models (DEMs), geographical information systems (GIS), and photograph processing software (Carrara and Pike 2008). These techniques can rapidly analyze spectral, geologic, and hydrologic maps to create regional mass-wasting inventories and assessments (e.g., Eeckhaut et al. 2011; Neuhäuser et al. 2012).

Semiautomated, supervised classification techniques have successfully produced inventories of mass-wasting candidates (Barlow et al. 2006; Borghuis et al. 2007; Moine et al. 2009; Martha et al. 2010). The inventory area is divided into training and evaluation areas. The

Published online: 11 April 2013

statistical properties of inputs in mass-wasting and non-mass-wasting classes are computed in the training area, which guide classification in the evaluation area. Evaluation effectiveness is often recorded as the percent of correctly identified mass failures compared to a field survey or air photo interpretation inventory; for example 60 % of debris flows (Barlow et al. 2006), 39 (Borguis et al. 2007), 26 (Moine et al. 2009), 69 (Martha et al. 2010), and 40 % of landslides (Neuhäuser et al. 2012). However, mass-wasting visibility, classification inputs, and the evaluation metric source differ by inventory thus, the evaluation usefulness reported as a percent are not fully comparable between studies.

Inventories can differ by inputs and the segmentation method used to delineate homogenous objects. Recent efforts commonly rely upon satellite imagery instead of the aerial imagery used in air photo interpretation (Nichol and Wong 2005; Barlow et al. 2006; Borguis et al. 2007; Martha et al. 2010). Normalized difference vegetation index maps created from imagery are used to infer areas with sparse or no vegetation, a potential indicator of mass-wasting scars (Barlow et al. 2006; Martha et al. 2010). This vegetation index ranges from −1 to 1 and values above 0.2 typically indicate vegetation present. Slope, aspect, hillslope curvature (Barlow et al. 2006; Van Den Eeckhaut et al. 2007), and water flow parameters (Martha et al. 2010) are derived from DEMs to determine the characteristic form of mass-wasting types.

Image segmentation by the spectral values of individual pixels is ineffectual when not combined with additional parameters (Barlow et al. 2006). Image segmentation using object-oriented analysis can be successful, since it incorporates not just individual pixel values but properties of data in adjacent areas (e.g., Martha et al. 2010). Image objects are still, in part, delineated by homogeneity of adjacent pixel spectral values, but other information, such as the objects' shape, texture, and size also determine the final segmentation. Object-oriented analysis incorporates the morphometrics of objects pertinent to debris flows, such as their total area (Barlow et al. 2006) and stream order (Martha et al. 2010), which may improve the subsequent classification of debris flow candidates by limiting false positives.

Geologic and geomorphic setting

Debris flow inventories were developed for five catchments (C1 to C5) totaling 269 km^2 in the southern Appalachians of western North Carolina (Fig. 1). The Appalachian Mountains were assembled by a series of convergent tectonic collisions approximately 1,200 to 260 million years ago with minor uplift during the Mesozoic and Cenozoic (Hatcher 1978; Gallen et al. 2013). The southeastern portion of the Great Smoky Mountains—the location of the five study catchments—is positioned on the southern limb of the Alum Cave Synclinorium formed of numerous second-generation, westward-trending folds and faults (Hadley and Goldsmith 1963). Present-day topography is characterized by rounded mountaintops, and deep valleys with steep slopes. Elevation ranges from 579 to 1,186 m and the mean slope is 28 ± 9 °. Mountain denudation occurs primarily through soil creep, in situ weathering of bedrock, river incision, and mass-wasting (Southworth et al. 2005; Jungers et al. 2009). Glaciation has not impacted the topographic signatures of these processes, since this region was not glaciated in the Pleistocene (Hadley and Goldsmith 1963). The ability of the range to maintain rugged topography despite the cessation of major uplift was explored by Matmon et al. (2003) who concluded that the Smoky Mountains are tending towards a steady state, given the similar erosion rates between ridge crests and drainage basins of 28 ± 8 mm × ky^{-1}. Similar erosion rates, including throughout the Oconaluftee basin (Fig. 1c), indicate that the area is in a state of dynamic equilibrium (e.g., Hack 1975), such that landforms adjust in short time steps so that erosion is consistent throughout the range over long time scales.

The five catchments are drained by the Oconaluftee River, which flows west via the Tuckasegee River, ultimately draining into the Gulf of Mexico via the Little Tennessee, Tennessee, Ohio, and Mississippi Rivers. Catchment streams are mixed bedrock-alluvial channels with pebble to boulder sediment. Streams flow over Precambrian bedrock composed predominantly of metamorphosed sedimentary rocks of the Ocoee Supergroup, along with gneiss, granodiorite, and amphibolite of the Grenville Basement Complex (Ygb in Fig. 2; Southworth et al. 2005). Within the Ocoee Supergroup, streams flow over rocks of the Anakeesta Formation (Za), principally slate, metasiltstone, and phyllite. Southworth et al. (2005) propose that the Copperhill Formation and Thunderhead Sandstone are the same unit, characterized by massive, graded beds of coarse-grained metasandstone interbedded with metasiltstone, thus these units are treated as one (Zct) in this study. Longarm Quartzite (Zl) outcrops adjacent to the Grenville Basement Complex in basins C3 and C4. Additionally, Southworth et al. (2005) mapped surficial deposits, including large debris fans (Qd) composed of expansive deposits of boulder diamict, and a historical debris flow unit (Qdf) that includes the initiation zone, track, and often the depositional area of the boulder diamict and transported vegetation. Debris flows begin most often atop the Anakeesta, Copperhead, and Thunderhead bedrock units and especially in areas where the regolith is less than a meter thick (Bogucki 1976; Southworth et al. 2005).

Debris flows have occurred in the Smoky Mountains for at least the last several tens of thousands of years and were especially frequent during the late Pleistocene and early Holocene (Kochel 1990). Bedrocks foliation and dip planes of the second-generation folds on the Alum Cave Synclinorium are especially prone to mass failure. Thick vegetation helps to stabilize soil, saprolite, and residuum on steep slopes. The shallow depth of regolith atop steeply dipping beds encourages failure when the soil cohesion and tensile strength of vegetation are surpassed by increases in soil pore pressure and/or shear stress from a moving debris flow (Southworth et al. 2005). Increases in hydrostatic pressure in preferential flow paths developed in the soil following intense precipitation may be an additional cause of mass-wasting in the region (Woodruff 1971). Mean annual precipitation in the southern Appalachians ranges from 1 to 2.7 m with snowfall accounting for 5 % of the total precipitation (Neary and Swift 1987). Precipitation intensities of 125 to 560 mm × day^{-1} have resulted in debris flows in the southern Appalachians (Witt 2005). The return period of a storm that delivers this threshold precipitation to the region is 10 years (Hershfield 1961); although Bogucki (1976) indicated that at least a 100-year storm was required to cause debris flows here. Debris flow recurrence in first-order catchments of the Smoky Mountains is estimated to be between 400 to 1,600 years (Kochel 1990). Southworth et al. (2005) summarize the known years of rainfall events that have resulted in debris flows in the Smoky Mountains prior to completion of their field work: 1938, 1940, 1942, 1943, 1951, 1956, 1967, 1971, 1975, 1984, and

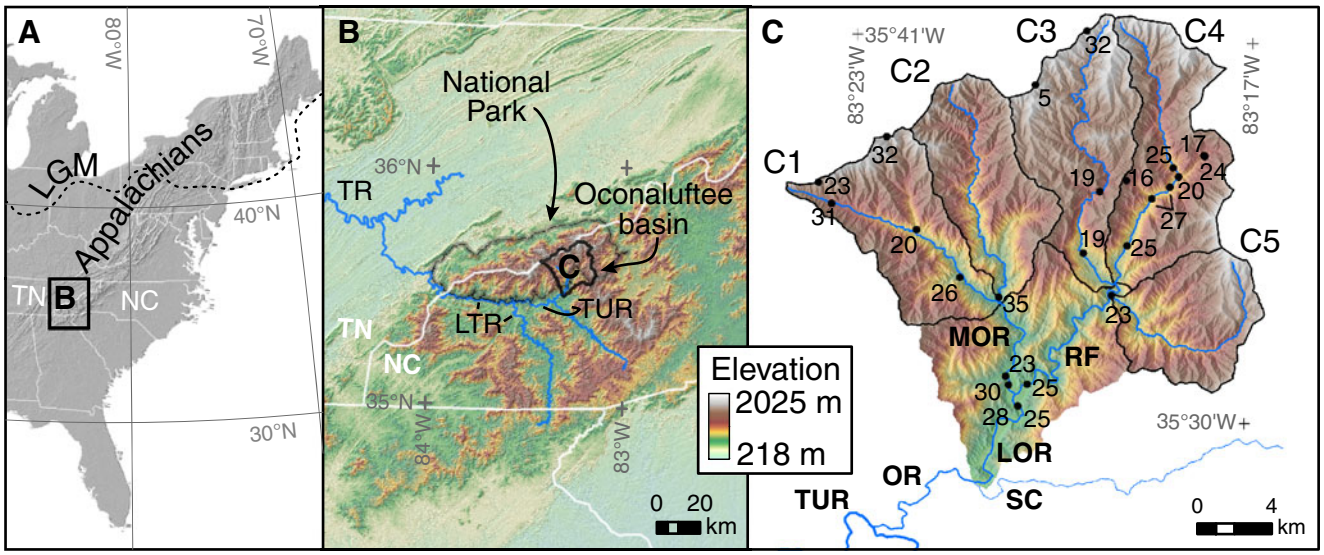

Fig. 1 **a** The southern Appalachian Mountains are located south of the Laurentide ice sheet margin during the last glacial maximum (*LGM*) and include parts of North Carolina (*NC*) and Tennessee (*TN*) (Dyke et al. 2002). **b** The Oconaluftee catchment in the Great Smoky Mountains National Park drains into the Tuckasegee (*TUR*), Little Tennessee (*LTR*), and Tennessee Rivers (*TR*). **c** C1 and C2 drain to the Middle Oconaluftee River (*MOR*). C3, C4, and C5 drain into the Raven Fork River (*RF*). The lower Oconaluftee River (*LOR*) basin above Soco Creek (*SC*), RF, and LOR are not included in analyses. Points and values are the locations of ^{10}Be basin-averaged erosion rates in mm×yr^{-1} from Matmon et al. (2003)

1993. Three known debris flows in adjacent first-order catchments occurred in 2011 during this study.

Methods

Two debris flow inventories were conducted and evaluated: the entirety of the five catchments—the "Catchment Inventory" and the portion of the catchments that drain to debris flow-dominated channels—the "A_{df} Inventory." The extent of the latter inventory is the area that drains to A_{df}, which is the transition from debris flow- to fluvial-dominated channel processes. This point is approximated using trends of drainage area (A) versus slope (S) in log-log space (AS Plots). Relationships between A and S have been used to indicate the landscape extent of dominant sediment detachment and transport processes (Montgomery and Foufoula-Geogiou 1993; Stock and Dietrich 2003; Tarolli and Dalla Fontana 2009). Streams in the Oconaluftee River basin were selected for AS Plot analysis if their drainage area is within the magnitudes of A_{df} of rivers throughout the world analyzed by Stock and Dietrich (2003).

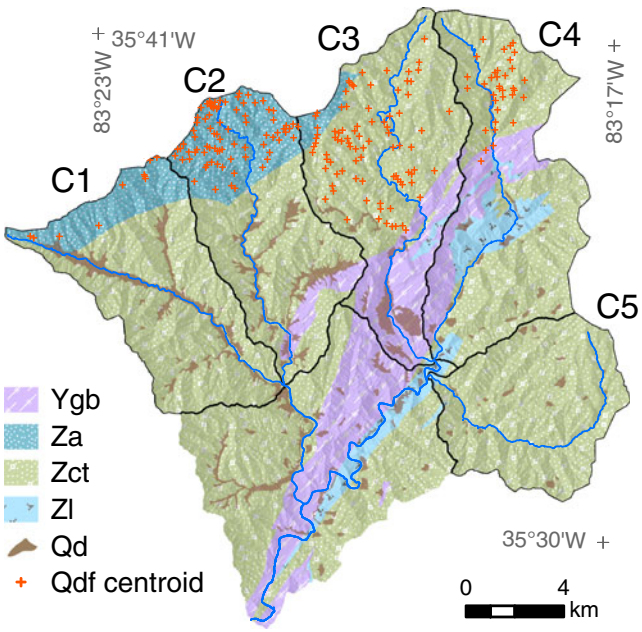

Fig. 2 Bedrock is generalized into the Grenville Basement Complex (*Ygb*), Anakeesta Formation (*Za*), the Copperhill Formation and Thunderhead Sandstone (*Zct*), and the Longarm Quartzite (*Zl*). Surficial deposits include debris fans (*Qd*) and debris flows (*Qdf*). See text for map unit descriptions. Geology mapped by Southworth et al. (2005)

The two inventories were created with a supervised classification algorithm so that debris flow identification capability can be tested when the area is limited to drainages of A_{df}. The outputs of the inventories are maps of debris flow areas that primarily include the head and track of historical debris flows. The debris flow head, track, and toe are considered as one unit because it is difficult and often erroneous to attempt to distinguish these areas (Malamud et al. 2004). The percent of debris flow and non-debris flow areas in a recent US Geological Survey map (Southworth et al. 2005) of historic debris flows that intercept debris flow and non-debris flow classed areas, respectively, was used for evaluation to compare the proficiency of the two inventories.

Data

Topography, imagery, and geologic datasets were used in the inventories and analyses. Topography was modeled with a bare-earth lidar (light detection and ranging) point cloud collected by the North Carolina Flood Mapping Program in April 2005 (North Carolina Flood Mapping Program 2011). The point cloud has a density of 0.41 points m^{-2} in the study area and represents the ground surface. Following Mitasova and Mitas (1993), our interpolation method, regularized spline with tension, was used to construct a DEM with a 4 m horizontal resolution. Topographic

derivatives were computed following Mitasova and Hofierka (1993) and are introduced first with the following simplifying notations:

$$f_x = \frac{\delta z}{\delta x}, f_y = \frac{\delta z}{\delta y}, f_{xx} = \frac{\delta^2 z}{\delta x^2}, f_{yy} = \frac{\delta^2 z}{\delta y^2}, f_{xy} = \frac{\delta^2 z}{\delta x \delta y} \quad (1)$$

and:

$$p = f_x^2 + f_y^2 \quad (2)$$

Slope angle, γ [degrees]; aspect, α [degrees]; profile curvature, K_s [m^{-1}]; and tangential curvature, K_t [m^{-1}] were computed from the DEM, also with a resolution of 4 m, as:

$$\gamma = \arctan \sqrt{f_x^2 + f_y^2} \quad (3)$$

$$\alpha = \arctan \frac{f_y}{f_x} \quad (4)$$

$$K_s = \frac{f_{xx} f_y^2 - 2 f_{xy} f_x f_y + f_{yy} f_x^2}{p\sqrt{(p+1)^3}} \quad (5)$$

$$K_t = \frac{f_{xx} f_y^2 - 2 f_{xy} f_x f_y + f_{yy} f_x^2}{p\sqrt{p+1}} \quad (6)$$

The DEM and topographic derivatives were created with Geographic Resources Analysis Support System (GRASS) GIS (GRASS Development Team 2011). A normalized difference vegetation index map was created from a National Aerial Photography Program 3-band infrared color-composite photograph with a 1 m resolution taken when trees were leafless in 1998. A bedrock and surficial geology map of the Smoky Mountains was created by the United States Geological Survey (USGS) prior to this study that includes a debris flow map unit delineated using the 1998 National Aerial Photography Program photograph (Southworth et al. 2005). Geologic map units were drawn on base maps with a scale of 1:24,000 from a compilation of previous maps, aerial photography, landform interpretation with topographic maps, and observations from field traverses. The scale was reduced to 1:100,000 when the mapped data were digitized by the USGS.

Stream selection for area–slope plot analysis

The streams that were included in *AS* Plot analysis were selected based upon stream order, since drainage area magnitude is central to the dominant channel process. Streams were selected from the entire modeled drainage network with the DEM, using multiple flow directions, which provides improved representation of convergent and divergent flow in comparison to unidirectional modeled flow (Quinn et al. 1991). Streams were defined as initiating at a drainage area threshold of 10^{-4} km^2. Drainage pathways with accumulation areas near this threshold are not channelized, but small areas were included so that the process regions throughout a catchment could be identified. Field observations of colluvial channels were observed in the field near drainage areas of 0.05 km^2; debris flows can initiate in colluvial channels (Wooten et al. 2008), and an average drainage area of 0.08 km^2 for initiation of perennial flow in small basins of the southern Appalachians has been determined (Rivenbark and Jackson 2004).

Streams with an order number of 6 following the notation of Strahler (1952) were included in the *AS* Plot analysis. This order was chosen because these streams are within the range of drainage area magnitudes where the transition from alluvial to debris flow-dominated channels has been observed in other rivers (Fig. 3). There are 32 order 6 streams in the five study catchments that are within the range of A_{df} detected in other rivers throughout the world (Fig. 4). Order 6 streams were extended from the outlet of the Oconaluftee River to the ridge for analysis. Streams with a lower order can be excluded from analysis since they are tributaries of the higher order streams where the transition is more likely to be found.

Delineation of the extent of channels dominated by debris flows

A and *S* were extracted from the DEM along selected streams at every 2 m increase in elevation and log-bin averaged with the ArcGIS (ESRI 2011) and MATLAB (MATLAB 2009) extension, Stream Profiler (Wobus et al. 2006). Profiles were smoothed using a 10 m moving window along the stream so that logjams, footbridges, and lidar vertical errors minimally affected the *AS* Plot values.

Signatures of the dominant upstream process were identified in *AS* Plots. Montgomery and Foufoula-Geogiou (1993) approximated the regions in *AS* space where the following landforms that have characteristic sediment transport processes exist: hillslope, unchanneled valleys, debris flow-dominated channels, and alluvial channels (Fig. 5). The interface of hillslope processes and debris flow-dominated channels, the critical drainage area (A_c), often coincides with the transition between divergent and convergent topography and theoretically occurs at a reversal of *AS* trend gradient in small drainage areas. However, due to noise in DEMs, the signature of this transition is typically seen as an inflection point where the *AS* trend gradient becomes more negative (Tarboton 1990; Ijjasz-Vasquez and Bras 1995). Another inflection point marks the transition from debris flow-dominated to alluvial channels (A_{df}), often where reach-average slope decreases below 0.03 to 0.10 $m \times m^{-1}$. This typically coincides with drainage areas of 0.1 to 1 km^2, dependent upon climate and basin geology (Seidl and Dietrich 1992; Montgomery and Foufoula-Geogiou 1993; Stock and Dietrich 2003). The debris flow-dominated region, when it is present, is bound by A_c and A_{df} and appears curved in *AS* Plots, which is in contrast to the power law that describes alluvial channels (Stock and Dietrich 2003).

An expression has not been determined for channels above A_{df} (Stock and Dietrich 2003). Below the scaling transition, Howard (1994) and Whipple and Tucker (1999), for example, describe stream incision into bedrock, $\delta z/\delta t$ [$m \times y^{-1}$] by:

$$\frac{\delta_z}{\delta_t} = U - KA^m S^n \quad (7)$$

where U is rock uplift rate relative to base level [$m \times y^{-1}$], K is rock erodibility [$L^{1-2m} \times y^{-1}$], A is drainage area [m^2] as a proxy for

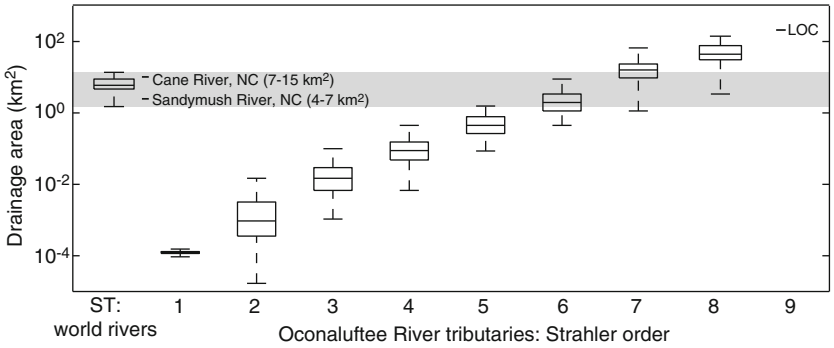

Fig. 3 The drainage area of tributaries by Strahler order. The scaling transition between alluvial and debris flow-dominated channels (*ST*) of rivers throughout the world (*gray band*), including two in North Carolina, was compiled by Stock and Dietrich (2003). Strahler orders below the gray area, *1* thru *5*, are less likely to contain the scaling transition

discharge, L is total bedrock stream length [m], S is channel slope [m×m^{-1}], and m and n are empirical values often referred to as the area and slope exponents, respectively. In steady-state landscapes, where $\delta z/\delta t=0$, channel slope is approximated with:

$$S = \left(\frac{U}{K}\right)^{1/n} A^{-m/n} \tag{8}$$

and in areas of uniform uplift and rock erodibility:

$$S = k_s A^{-\theta} \tag{9}$$

where k_s, $(U/K)^{1/n}$ in Equation 8, is referred to as the steepness index and θ, m/n in Equation 8, as the concavity index. In the Smoky Mountains, we assume that localized uplift is likely nonexistent or uniform such that it can be disregarded as required for Equation 9.

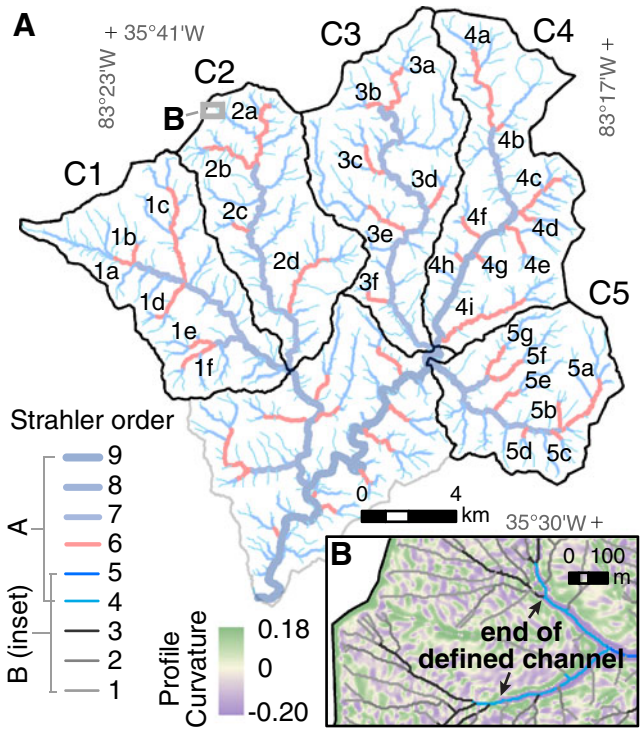

Fig. 4 **a** 32 Strahler order 6 streams within the five study catchments were analyzed in *AS* space for a scaling transition. **b** Fourth-order headwater streams extend to the uppermost limit of defined channels and reside near the 0.05 km^2 area threshold where channel heads were observed in the field

The process signatures described above were used to bound regression limits in *AS* space. Power laws were used in all regressions for comparing all *AS* trends, but are applicable only to alluvial channels. A trend with low θ at small drainage areas that transitions to high θ at its downstream extent is defined as the hillslope region. The debris flow-dominated portion is defined as the *AS* trends where θ increases monotonically. The profile downstream of the termination or absence of a monotonically increasing θ is the alluvial channel region.

AS scaling analysis can be complicated by knickpoints, which are defined as highly convex reaches in longitudinal profile of a channel, and can include waterfalls or cascades (Fig. 6; Stock and Dietrich 2003; Clark et al. 2005; Foster and Kelsey 2012). Deviations from steady-state topography, such as knickpoints, and variation in rock erodibility introduce anomalous k_s and θ values. The evolution of knickpoints—stationary or propagating upstream—and their origin—autogenic or regional—introduces further spatial variability in *AS* scaling. Knickpoints propagate upstream when both critical shear stress (τ_c) overcomes actual shear stress (τ_o) on the knickpoint lip and τ_o overcomes τ_c at the knickpoint base (Gardner 1983). Knickpoints that degrade at their lip are further lowered, forming a convex zone called the drawdown reach (Gardner 1983). Autogenic knickpoints form upon resistant lithologies or due to stream power contrasts at tributary junctions (Crosby and Whipple 2006). Regional uplift and base level fall can also cause knickpoints to form at the interface of equilibrated and disequilibrated landscapes (e.g., Clark et al. 2005; Crosby and Whipple 2006). *AS* scaling variations due to regional uplift is not a consideration in the tectonically

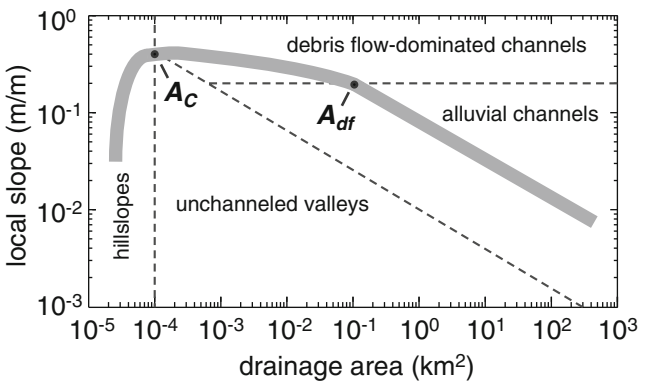

Fig. 5 Scaling in log-bin average drainage area versus channel slope. Breaks at process transitions are identified. Modified by permission of American Geophysical Union from Montgomery and Foufoula-Geogiou (1993)

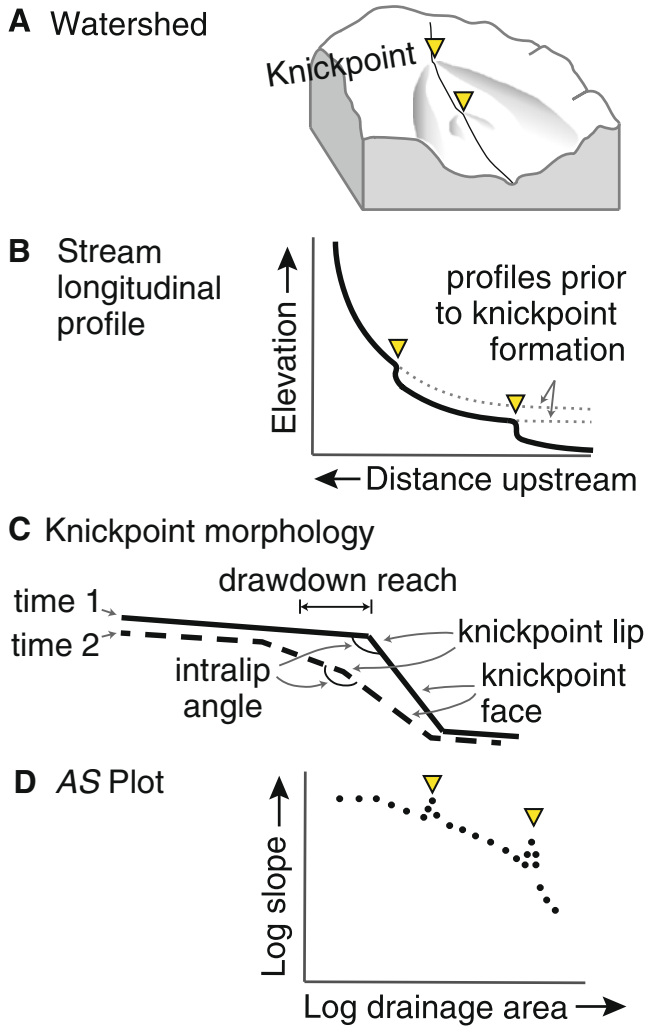

Fig. 6 **a** Hillslopes adjacent to knickpoints are steepened since incision is more advanced downstream. **b** Projection of stream profiles illustrates stream elevation prior to the formation of the knickpoint. **c** Time series of knickpoint degradation, modified from Gardner (1983). **d** Process regions in *AS* Plots can be interrupted by knickpoints that appear as jumps in stream slope

quiescent Appalachians, but hillslope instability due to propagating knickpoints occurs within the region (Gallen et al. 2011).

Whatever process(es) a single or set of knickpoints owe their origin to, these features can affect identification of debris flow-dominated channels and in part explain spatial variation in *AS* scaling (Fig. 6). We therefore bounded regression limits at points of major knickpoints, in a manner similar to Foster and Kelsey (2012), in addition to process signature regression bounds. Knickpoints were identified at points along the channel longitudinal profile with a noticeable convexity, a measureable change in slope of at least 0.02 over 500 m, and normalized k_s values that peak at a minimum of 70.

The extent of debris flow-dominated channels—the area that drains to A_{df}—needed for this mass-wasting inventory technique also includes the hillslope region in catchment headwaters where debris flow initiate as landslides. To evaluate the effectiveness of DEM detection of A_{df} and the extent of debris flow-dominated channels, we compare catchment metrics to landscape evolution state proposed by others; primarily dynamic equilibrium proposed by Hack (1975) and applied to the Smoky Mountains by Matmon et al. (2003). Hypsometry, relief, and bedrock and knickpoint distributions across the five catchments were determined since these metrics can provide insight into the evolution state of a landscape (Hack 1975; Howard 1994). Local relief was calculated as the range in elevation in moving circular windows with a 50 m radius.

Identification of debris flows from topographic parameters and imagery

The Catchment and A_{df} Inventories differed only by the extent of the inventory area. The same input types and classification algorithm were used to create the inventories. Texture maps were used as classification inputs since local variations, such as shadows and vegetation, may influence the statistical characterization of classes (Moine et al. 2009; Martha et al. 2010). Textural features, as defined and applied by Haralick et al. (1973), are computed as the co-occurrence frequency of gray level pixel value pairs separated by a given distance in a matrix of a given size. The pairs within the moving neighborhood matrices are assigned by a displacement vector between two pixels as a direction, commonly 0, 45, 90, and 135 °. The texture algorithm used in GRASS GIS uses these directions and allows for numerous textural feature types to be calculated. The following texture maps of inputs were computed in 144 m² matrices containing 3 by 3 arrays of 4 m² cells in the study area: (1) slope entropy, a measure of the uncertainty of a variable, (2) profile and (3) tangential curvature entropy, and (4) normalized difference vegetation index sum average. These textual features were calculated as:

$$\text{Entropy} = -\Sigma_i \Sigma_j p(i,j) \log(p(i,j)) \tag{10}$$

and:

$$\text{Sum average} = \sum_{i=2}^{2N_g} i p_{x+y}(i) \tag{11}$$

where $p(i,j)$ is the spatial-dependence matrix with paired input values i and j, N_g is the number of distinct gray levels in the matrix, and x and y are the number of columns and rows in the matrix, respectively (Haralick et al. 1973). Texture maps were equally weighted and scaled from 0 to 255 for classification. This scale was necessary, as the GRASS GIS texture, segmentation, and classification algorithms are designed for 8-bit imagery input.

The texture maps were used to classify the two inventory areas into “debris flow” and “non-debris flow” candidate classes using a supervised classification workflow. These classes were determined as a probabilistic combination of subclasses in a Gaussian mixture distribution model and segmented using a Bayesian approach, following Bouman and Shapiro (1994). The algorithm began testing clustering at ten subclasses for each class and iteratively reduced this number until an optimal number of subclasses containing signatures similar to training area classes were reached. Subclass signatures were defined by the means and covariance matrices of the texture map inputs during the first step of the classification workflow—the training stage. Catchment C2, the 59.8 km² Bradley Fork catchment, was chosen as the training area because of the abundance of debris flow scars visible on aerial photos.

The second step, segmentation, was carried out using sequential maximum a posteriori (SMAP) estimation, a procedure typically

Table 1 Summary statistics for catchment trunk streams

	Total area [km^2]	Hypsometric index	A_{df} Drainage area [km^2]	A_{df} Channel slope [m×m^{-1}]	Stream length below scaling transition [km]	Knickpoint elevations [m]
C1	62.7	0.45	13.1	0.09	17.2	1,044, 1,181, 1,461
C2	59.8	0.49	21.4	0.04	17.6	835, 975, 1,093, 1,260
C3	51.3	0.58	35.3	0.03	22.8	917, 977, 1,085, 1,173, 1,582
C4	53.7	0.49	21.2	0.03	22.1	1,042, 1,199, 1,426
C5	41.8	0.47	5.86	0.05	20.0	947, 1,339

applied to multispectral image analysis (McCauley and Engel 1995). SMAP was chosen for its ability to minimize large misclassified areas as well as to incorporate neighboring pixel values in segmentation, thus incorporating contextual information. Lastly, debris flow

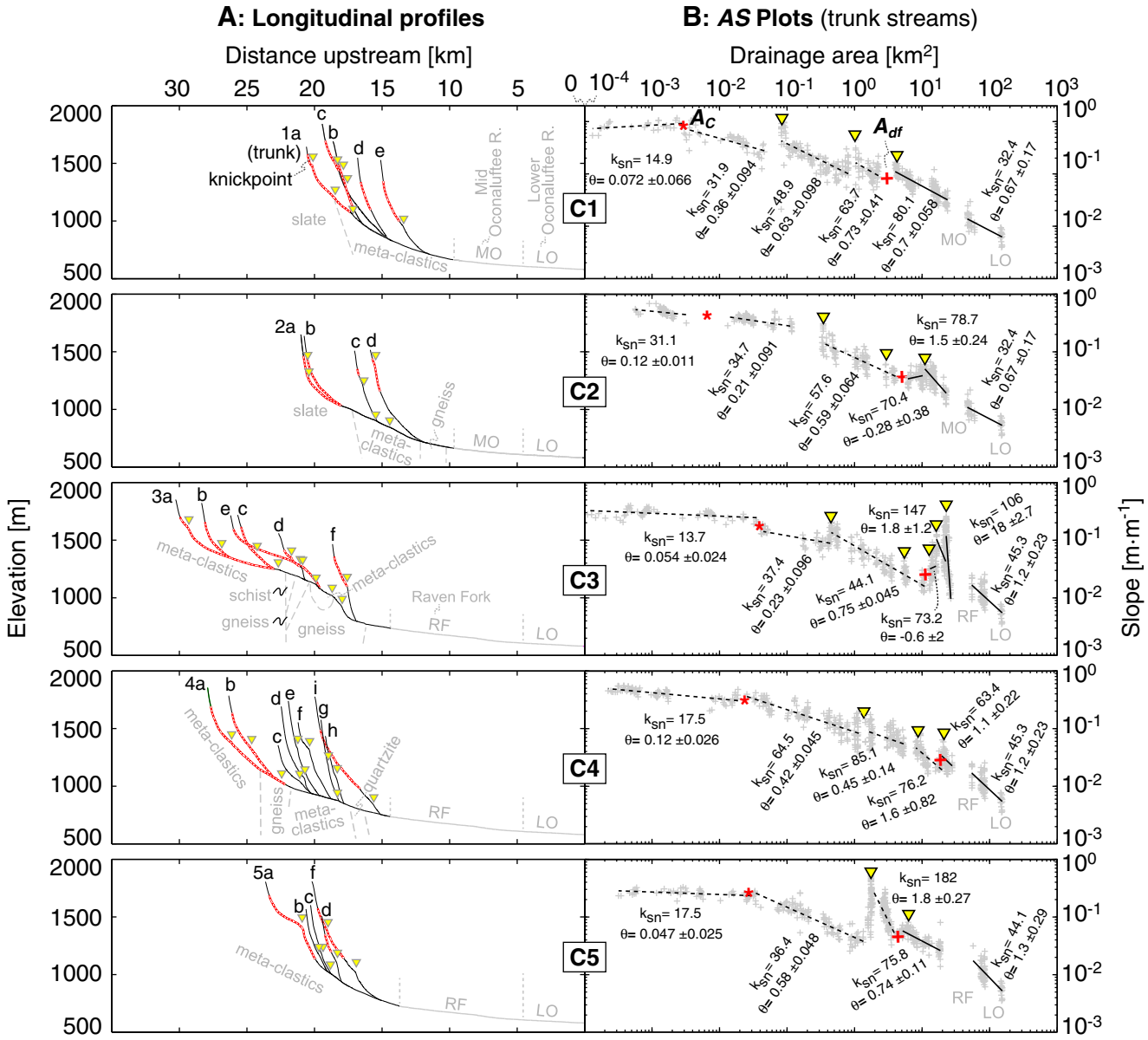

Fig. 7 **a** Profiles of trunk channels and their 6th-order tributaries from the five study catchments. Extent of debris flow-dominated channels is highlighted in *red* and bounded by A_c and A_{df}. Tributaries 1f and 5e are not shown since they are similar to 1e and 5b, respectively. Subsurface bedrock from Southworth et al. (2005) and Matmon et al. (2003). **b** Regressions of the curved region (*dashed lines*) and power law region (*solid lines*) of trunk channels *AS* values at 2 m contours (*gray crosses*)

candidates were reclassed as "non-debris flow" if they did not have the following morphometric criteria similar to debris flows in the training area: slopes of 8 to 44 ° and a planimetric area of 0.005 to 0.5 km². Barlow et al. (2006) used a lower limit of 0.01 km² since smaller scars are difficult to detect with the DEM and satellite imagery they used. However, the higher resolution of the lidar DEM and aerial photography of this study permits a smaller minimum area. Further, the smaller size of debris flows in this study demands a lower minimum debris flow area in order to identify many of the flows.

The process outlined above: multiresolution contextual segmentation of sites with similar topographic derivatives and normalized difference vegetation index textures, classification of segments into two classes, and reclassification based upon known morphometrics, produced a map of debris flow candidates that can be evaluated against the baseline USGS map. The percent of debris flow and non-debris flow areas in the USGS map that intersect debris flow and non-debris flow classed areas, respectively, was used to compare the proficiency of the two inventories.

Results

The extent of debris flow-dominated channels was determined with *AS* Plot scaling analysis. This produced a reduced area for the A_{df} Inventory. Proficiency is higher in the A_{df} inventory when classification inputs are restricted to the drainages of debris flow-dominated channels.

AS Plots and catchment metrics

Multiple geomorphic process regions, including debris flow-dominated channels, were identified in the *AS* Plots of many of the selected streams. A hillslope region is present in *AS* Plots of all streams with drainage areas of 0.02 to 0.04 km², which is near the upstream limit of defined channels in the DEM and channel heads observed in the field. The scaling transition between alluvial and debris flow-dominated channels is observed in all trunk channels. A_{df} ranges between slopes of 0.03 and 0.09 and drainage areas of 5.86 and 35.3 km², which are within values observed in channels throughout the world (Table 1; Fig. 7; Stock and Dietrich 2003). The maximum k_{sn} value in each trunk channel occurs near the transition that was placed at the maximum θ. The elevation of debris flow-dominated channels is similar in catchment tributaries; although not all tributaries contain a debris flow-dominated section, such as tributaries 4c–4 h, where there was no monotonically increasing θ. Knickpoints are most frequent around 1200 m, which created the need for multiple regressions.

The upstream drainage area of A_{df} totals 128 km², which is 52 % smaller than the entire study area of 269 km² (Fig. 8). All catchments have debris flow-dominated tributaries downstream of the A_{df} in trunk streams, with the exception of C2. All of the USGS-mapped debris flows and the majority of debris fan deposits are located upstream and downstream of A_{df}, respectively. The uppermost point of debris fans is significant to the location of the A_{df} since the fan deposits, primarily attributed to debris flows in the late Pleistocene and early Holocene, show evidence of having been reworked by fluvial action (Leigh and Webb 2006; Southworth et al. 2005). The mapped historical debris flows in the area occur in tributary streams, though the track sometimes extends into the trunk valley. Thus, the fans represent the debris flow material storage site, in large volumes in the area, but not the initiation or deposition site of recent debris flows.

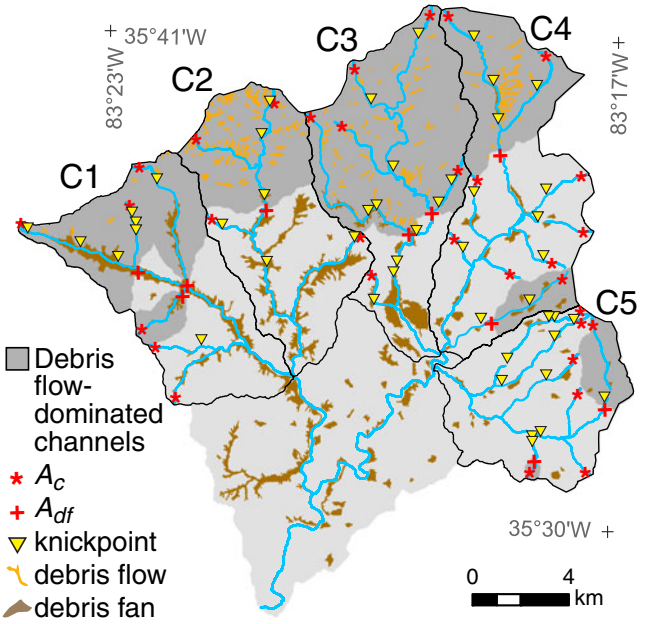

Fig. 8 The extent of debris flow-dominated channels includes the hillslope region in small drainage areas near ridges. Debris flows and fans mapped by Southworth et al. (2005)

The upstream drainage area of A_{df} is positively correlated with the hypsometric index of the catchments (Table 1). The hypsometric index is highest in C3 and decreases east and west through the other catchments. C3 and C5 have hypsometric curves that are unlike steady-state landscapes, due to the prevalence of high elevations above areas locally referred to as "the Gorge" and Bunches Creek falls, respectively (Fig. 9). Local relief is highly variable, although two types were observed—areas with low relief and high elevation (Type 1 relief), and areas with high relief adjacent to rivers (Type 2 relief) (Fig. 10). Type 1 relief is most common within the drainage area of A_{df}. Type 2 relief is most common near and below A_{df}. Many of the USGS-mapped debris flows in C3 and C4 are within Type 2, where the debris flow initiation zone is at the upper extent of this relief type.

Classification input maps

The spectral and topographic classifiers are compared with the USGS debris flow map. Distinction between valleys, some ridges,

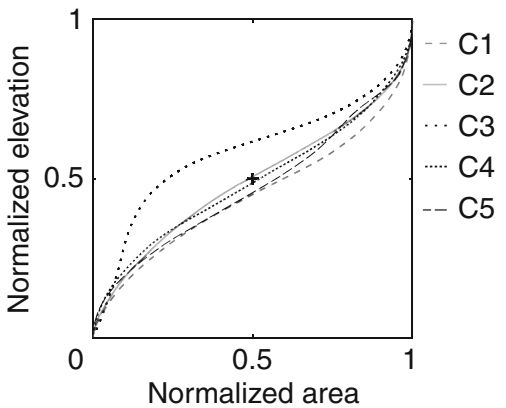

Fig. 9 Hypsometric curves of the five study catchments

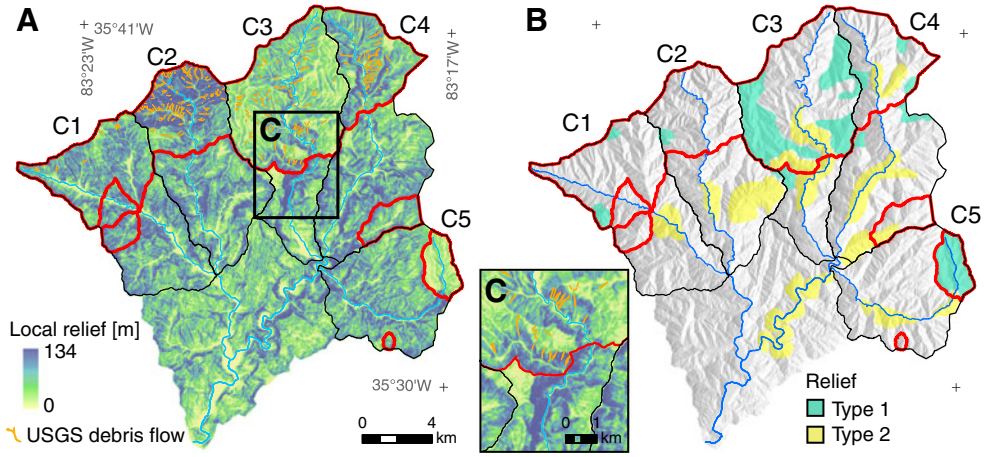

Fig. 10 **a** Relief calculated in moving windows with a 50 m radius. **b** Two relief types were observed: Type 1 at high elevations with low relief and Type 2 adjacent to channels with high local relief. **c** Many USGS-mapped debris flows are located in relief Type 2, especially in C4 and C3, shown here at the area locally referred to as "the Gorge"

and USGS debris flows is ambiguous based upon the 1998 aerial photo (Fig. 11a) and normalized difference vegetation index map (Fig. 11b). However, the coincidence between USGS debris flows and low sum average values is apparent in the texture maps created from the vegetation index map (Fig. 11c). Exposed soil and bedrock resulting from vegetation removal by debris flows is responsible for the low vegetation index values in the 144 m² texture feature neighborhoods in which this input was created. Valleys and ridges are less apparent, given the texture neighborhood size that is larger than many of these landforms are wide and possibly also due to sporadic vegetation.

The range of topographic hetero- and homogeneity was determined by low and high values of entropy, respectively. The USGS-mapped debris flows have a large range of hillside slope magnitudes (Fig. 11d). High slope entropy, indicating areas with similar slope magnitudes, often occurs at the lowest elevations of the USGS debris flow maps and decreases up the flow (Fig. 11e). Concave profile curvature in debris flow areas is concordant with debris flow initiation in areas of convergent drainage lines (Fig. 11f). Similar to slope entropy, the lower section of USGS-mapped debris flows have high entropy, as do channels, and the upper sections have low entropy (Fig. 11g). The low entropy values are likely due to vegetation flanking the flow scar that is included in the texture neighborhood in the more narrow upper sections of debris flows.

Classification results

Debris flows in the USGS debris flow map, Catchment Inventory, and A_{df} inventory cover 16.1, 24.3, and 11.6 km², respectively. The USGS map contains 65 debris flows, although it is difficult to quantify debris flow candidates in the two inventories created in this study since the classification algorithm appears to have clumped several flows. Debris flow candidates are concentrated near trunk streams in the Catchment Inventory, and within low-order catchments in the A_{df} Inventory (Fig. 13).

The inventories are evaluated in terms of "agreement" where USGS-mapped debris flow and non-debris flow areas correspond

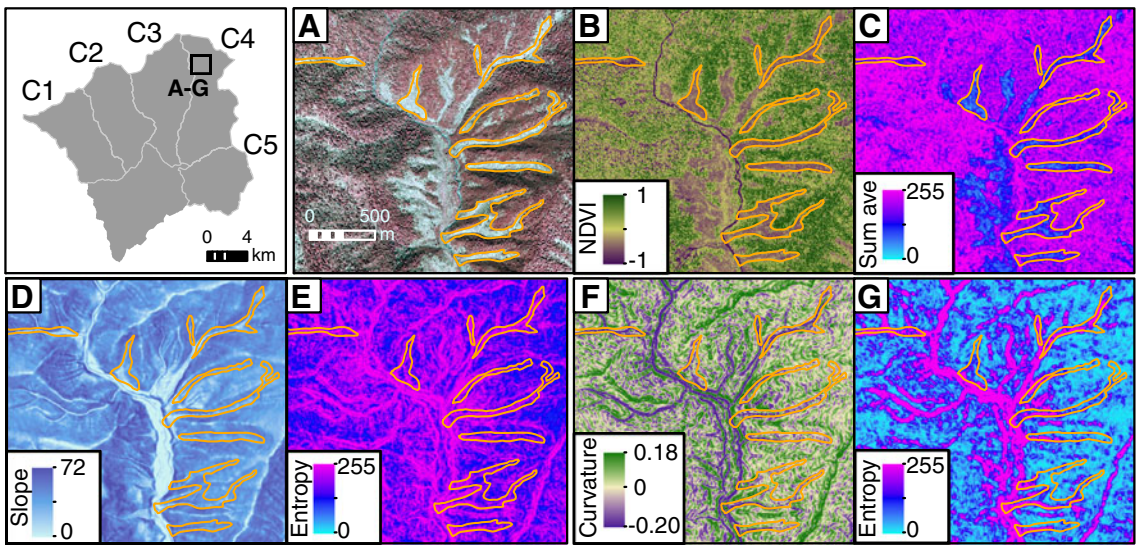

Fig. 11 **a** False color aerial photograph. **b** Normalized difference vegetation index (NDVI) calculated from aerial photograph. **c** Texture of NDVI calculated as sum average and scaled to 0 to 255. **d** Slope [degrees]. **e** Texture of slope calculated as entropy. **f** Profile curvature [m^{-1}]. **g** Texture of profile curvature calculated as entropy

to inventory classes and "disagreement" where they do not intersect. The terms true and false positive are not used in this evaluation, since inventory results were not field verified. Agreement calculated by the count of debris flows, where more than 25 % of the USGS-mapped debris flow was classified "is a debris flow", was 12 % higher in the A_{df} Inventory by area (Table 2).

Large tracts of disagreement are more prevalent in the Catchment Inventory compared to the A_{df} Inventory (Fig. 12a and a'). The coincidence of forest type and the drainage area of A_{df} is the primary cause for this (Fig. 13). The low normalized difference vegetation index entropy of hardwood forests was more strongly associated with the debris flow class in the Catchment Inventory, while the A_{df} Inventory was trained to associate high slopes with low vegetation index texture values. High vegetation index values coincide with spruce-fir and northern hardwood forests, which are common above 1200 m, and low values with oak, hickory, and montane cove forests found at lower elevations (Madden et al. 2004). Low texture values were characteristic of both low-elevation forests and debris flows. Thus reducing the extent of low-elevation forest in the A_{df} Inventory permitted finer resolution characterization of inputs for the subclass signatures to resolve vegetation index texture variations. This is the reason why large tracts of low vegetation index texture, such as shown in fig. 13a', were correctly classified as non-debris flow in the A_{df} Inventory. Similar phenomena occurred with the other inputs; for example, slope and curvature textures in debris flow areas and below A_{df} were both high. Characterization resolution for these inputs also increased when the inventory was limited to areas that drain to A_{df}.

Small USGS-mapped debris flows were often not identified as such in the Catchment Inventory, though the lowest section was recognized in the A_{df} Inventory (Fig. 12b and b'). This is primarily due to the high texture values common in the lower portions of USGS-mapped debris flows.

Both inventories have high agreement for large USGS-mapped debris flows, though it is noticeably higher in the A_{df} Inventory (Fig. 12c and c'). The texture neighborhood was less influenced by boundary conditions in these larger areas, allowing for increased differentiation between classes.

Discussion

The role of debris flow-dominated channels in the evolution of the Oconaluftee River

An investigation into mechanisms that control the position of A_{df}, and thus the extent of debris flows, was motivated by the order of magnitude range in this parameter. Bedrock erodibility can be a first-order control upon landscape evolution, longitudinal profile form, and knickpoint development (Stock and Montgomery 1999).

Table 2 Comparison of inventory evaluation results

Inventory	Agreement by debris flow count [%]	Agreement by area [%]	
		Debris flow	Non-debris flow
Catchment	64	45	89
A_{df}	76	57	86

Local bedrock, debris flow, and knickpoint distribution indicate that this is the case in the Oconaluftee River basin. All catchments are predominantly underlain by metaclastics of the Copperhill Formation and Thunderhead Sandstone. While these units do contain siltstone, minor amounts of slate, and high dip planes susceptible to failure, none of the USGS-mapped debris flows are present on this map unit in C1 and C2. Conversely, debris flows occur almost exclusively upon these units in C3 and C4, indicating that there is an additional control upon debris flow initiation that varies spatially. The following paragraphs synthesize catchment metrics and the extent of debris flow-dominated channels. This synthesis relates channel and hillslope coupling with the mechanisms that determine the position of A_{df}.

The distribution of debris flows throughout the study area is in agreement with Matmon et al. (2003), who proposed that the southern Appalachians, and specifically, the Great Smoky Mountains, is in a state of dynamic equilibrium where high relief is maintained by isostatic rebound of a thick crustal root, and erosion of landscape elements adjust such that the area is down wasting at the same rate over long timescales. Stream incision is most advanced below the debris flow-dominated area, as indicated by high-relief zones adjacent to channels and concave-up longitudinal profiles. The advanced lowering of channels and hillslopes in C1 and C5 has resulted in a decreased extent of debris flow-dominated channels. In contrast, much of C2, C3, and C4 are debris flow-dominated catchments with less entrenched valleys and lower overall relief upstream from A_{df}, which corroborates their low hypsometric integrals. Less entrenched valleys and low relief are typically indicators of areas without debris flows, but comparison of knickpoint and hypsometry of these catchments with C1 and C5 indicate that these hillslopes are adjusting to conditions similar to those in adjacent catchments through increased debris flow activity.

A second mechanism is suggested by the relative positions of knickpoints and debris flows in comparison with those in studies by Crosby and Whipple (2006) in New Zealand and Gallen et al. (2011) in an area approximately 60 km south of the Smoky Mountains. In these studies, many debris flows are located close to and below knickpoints that are more directly caused by hillslopes adjusting to incising channels in the wake of upstream knickpoint propagation. In the Smoky Mountains, the cause of hillslope instability due to upstream knickpoint passage is less clear. Knickpoints cluster at approximately 1200 m in elevation, which coincides with the approximate locations of A_{df} and maximum steepness index. This implies that a locus of geomorphic response to base level fall, or another knickpoint origin, is centered at this elevation. Knickpoints above this elevation, as well as the lowering of the drawdown reach, will have first destabilized hillslopes adjacent to trunk channels, then up to ridges. Base level fall and/or propagating knickpoint are implicated by the presence of sharp knickpoints at similar elevations in tributaries, such as between tributaries 3a, 3b, 3d, 3e, and 3f; and 4a, 4b, 4e, and 4f (Fig. 4).

These mechanisms acting alone cannot fully explain landscape evolution of the Oconaluftee River basin, although a combination of these mechanisms produces a viable synthesis of the catchment metrics and the extent of debris flow-dominated channels. Drops in base level or other initiators of propagating knickpoints, along with lithologic differences, induce A_{df}

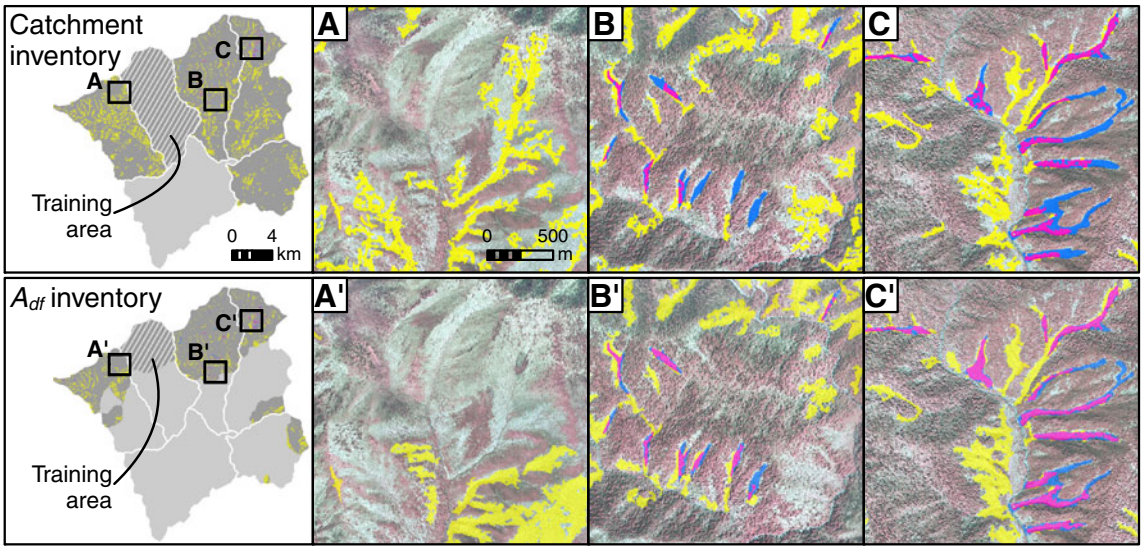

Fig. 12 Evaluation of the Catchment (*top row*) and the A_{df} (*bottom row*) inventories. Each column of insets, **a** and **a**′ for example, show the same location so that inventories can be compared. The base map is from the 1998 color-composite aerial photograph

variability. We attribute the debris flow-dominated extent in C2, which is intermediate in area, to the outcropping of landslide-prone slate throughout the headwaters. The reduced channel lowering and wider debris flow-dominated extent in C3 and C4 is the product of the outcroppings of gneiss and quartzite. These resistant lithologies impede headward stream (knickpoint) incision, resulting in a greater portion of the landscape being in disequilibrium. Debris flows are located upstream of the lithologically inhibited knickpoints of these catchments, in contrast to observations elsewhere. It is hypothesized here that the uppermost knickpoint of C3 and C4 have propagated to the stream power threshold more recently than C1 and C2. If this is true, the debris flows that are adjacent to the trunk streams throughout the catchment could be caused by local relief increases caused by propagating knickpoints that destabilized the hillslopes. The mechanisms that control the extent of debris flow-dominated channels remain unclear, yet indicators in the Oconaluftee do not violate characteristics of landscape evolution state and incision mechanisms proposed by others.

Inventories of debris flow-dominated channels

The historical debris flow prone portion of the landscape was delineated as the areas that drain to A_{df}. This landscape portion represents not only the hillslope process region where debris flows initiate, but also the debris flow-dominated channel region where moving flows cause geomorphic alteration and hazard to life and property. This signature persists in the non-glaciated southern Appalachians, thus we exploited this during the creation of a debris flow inventory.

A higher percentage of classes were correctly identified in the A_{df} Inventory than the Catchment Inventory. Removal of false positives eliminated many of the areas incorrectly identified by classification, though numerous errors of commission remained. Small gullies adjacent to tributaries are the largest source of this type of error. These features have similar curvature, slope, and normalized difference vegetation index values of debris flows. Borghuis et al. (2007) noted an analogous phenomenon when they found that the differences between mean size and the number of landslides classified using computer and manual methods is often due to differences in how landslides are grouped. Multiple debris flow tracks from

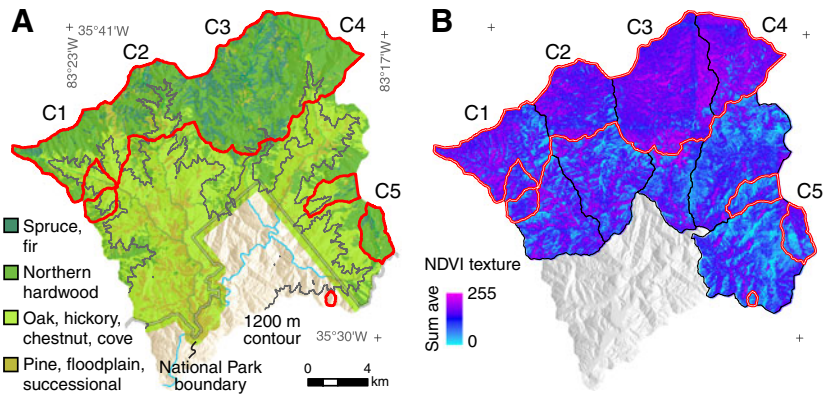

Fig. 13 **a** Vegetation forest classes mapped by Madden et al. (2004). **b** Normalized difference vegetation index (NDVI) texture of the five study catchments

adjacent valleys that intersect in the trunk valley typically comprise one track in manual delineation. However, patches of vegetation, false positive removal, or cell size and neighbor statistics can divide debris flows into numerous segments. Some of these features may be debris flows that were not identified during the USGS mapping effort. The large size and remoteness of some areas within the National Park, the thick forest canopy, the time since the last mapping effort, and the subjectivity of aerial photograph interpretation may result in omission of debris flows. New techniques, field verification, and improved understanding of an area's landscape evolution may reveal previously unmapped debris flows.

To our current knowledge, we see few limitations to the application of this technique where the debris flow topographic signature has been detected, which has been in basins throughout the world (Stock and Dietrich 2003). Little improvement between an A_{df} and Catchment Inventory may occur in some regions where topography is homogenous throughout the area, or where the extent of debris flow activity is found to encompass the original inventory area. Furthermore, the technique is applicable only for debris flow mass-wasting. As proposed by Barlow et al. (2006), a combination of inventorying techniques may be necessary where there are multiple mass-wasting types, due to dissimilarities in the physics of failure and morphology among types. Numerous other mass-wasting types were observed in Smoky Mountains, including debris slides and block topples, which may frequently occur with debris flows in dynamic equilibrium landscapes. This technique is also applicable to other debris flow detection methods. A classification algorithm was used in this investigation to quantitatively demonstrate the proficiency of this technique. Aerial photographic interpretation and field-based methods may also benefit by focusing on areas that exhibit the debris flow topographic signature. In the instance of the A_{df} Inventory in this investigation, more than half of the area in the five catchments exists outside of the debris flow-dominated region.

The signature of debris flows in the resolution of single mass failures at the scale of landscapes may be difficult to determine, given their small size, overprinting processes, and vegetation canopy (Van Den Eeckhaut et al. 2007). This is the case in the southern Appalachians, due to both millions of years of debris flow activity and complex forest canopy structure (Kochel 1990). For time scales smaller than debris flow recurrence interval, and at spatial scales equivalent to mass failures, the effects of debris flows on geomorphology and vegetation are detectable in the field and in aerial imagery for a period of years after the debris flow occurred. At scales outside these ranges, inventories may be incomplete, especially if vegetation is a highly weighted criterion of remote mass-wasting classification. Contextual inputs provide additional classifiers to negate issues of spatial scale limits in imagery, although landscape evolution context has often been ignored. Debris flow inventories of non-glaciated regions can benefit from incorporating landscape evolution scale processes into the inventory process.

Creation of inventory maps based upon known debris flows, without understanding the controls upon their parameters, is shortsighted. The hillslope evolution of the southern Appalachians and its connectivity to fluvial incision remains enigmatic. Further work to resolve the timing and mechanisms of knickpoint retreat, hillslope response, and the coupling of these two processes can further improve debris flow hazard reduction strategies. A comprehensive analysis of landscape evolution may not always be necessary for inventories that employ machine learning algorithms. However, limiting inventories to hillslopes that drain to debris flow-dominated channels focuses inventory efforts.

Conclusions

The order of magnitude variation in the drainage area of debris flow-dominated catchments in the Oconaluftee River basin emphasizes the need of catchment-scale investigations to determine the extent of debris flows. High relief and the lower bounds of debris flows mark the margin of the landscape that exhibits the debris flow topographic signature as predicted by the dynamic equilibrium landscape evolution state of the Smoky Mountains. Detection of debris flows in the mass-wasting inventory of this area was higher than the inventory conducted in the entirety of the study area. The A_{df} Inventory omitted lower valleys where topography markedly differs from higher elevations, which narrowed the classification input ranges to values that are representative of just the areas where debris flows occur. Many of the errors in both inventories were systematic, for example, in the locations of small gullies adjacent to streams and omission of debris flow heads, thus refinements to the classification algorithm may further improve inventory proficiency. Field verification may also benefit evaluation of this technique, as it is likely that the USGS map used for evaluation does not contain all historic debris flows. The suggested refinements and application to other areas will further assist the evaluation of this mass-wasting inventorying technique.

Acknowledgments

The authors wish to thank the National Park Service staff of the Great Smoky Mountains for their assistance; especially Paul Super, Benjamin Zank, Kris Johnson, Matt Kulp, and Keith Langdon. Field assistance was provided by Jacqueline S. Gronwald. Regional insight and technical guidance was provided by Scott Southworth, Michael Starek, Sean Gallen, Richard Ketelle, and Bill Weatherspoon. Reviews by Mauri McSaveney, Birgit Terhorst, and two anonymous readers greatly improved the manuscript.

References

Barlow J, Franklin S, Martin Y (2006) High spatial resolution satellite imagery, DEM derivatives, and image segmentation for the detection of mass wasting processes. Photogramm Eng Remote Sens 72:687–692

Bogucki DJ (1976) Debris slides in the Mt. Le Conte area, Great Smoky Mountains National Park, USA. Geografiska Annaler 58(A):179–191

Bouman CA, Shapiro M (1994) A multiscale random field model for Bayesian image segmentation. IEEE Transactions on Image Processing 3:162–177

Borghuis AM, Chang K, Lee HY (2007) Comparison between automated and manual mapping of typhoon-triggered landslides from SPOT-5 imagery. Int J Remote Sens 28:1843–1856

Brardinoni F, Slaymaker O, Hassan MA (2003) Landslide inventory in a rugged forested watershed: a comparison between air-photo and field survey data. Geomorphology 54:179–196

Carrara A, Pike RJ (2008) GIS technology and models for assessing landslide hazard and risk. Geomorphology 94:257–260

Clark MK, Maheo G, Saleeby J, Farley KA (2005) The non-equilibrium landscape of the southern Sierra Nevada, California. GSA Today 15:4–10

Crosby BT, Whipple KX (2006) Knickpoint initiation and distribution within fluvial networks: 236 waterfalls in the Waipaoa River, North Island, New Zealand. Geomorphology 82:16–38

Cruden DM, Varnes DJ (1996) Landslide types and processes. In: Turner AK, Schuster RJ (eds) Landslides: investigation and mitigation. Transportation Research Board, National Research Council, Washington D.C, pp 36–75

Dietrich WE, Wilson CJ, Montgomery DR, McKean J, Bauer R (1992) Erosion thresholds and land surface morphology. Geology 20:675–679

Dyke AS, Andrews JT, Clark PU, England JH, Miller GH, Shaw J, Veillette JJ (2002) The Laurentide and Innuitian ice sheets during the last glacial maximum. Quat Sci Rev 21:9–31
Eeckhaut M, Hervás J, Jaedicke C, Malet JP, Montanarella L, Nadim F (2011) Statistical modelling of Europe-wide landslide susceptibility using limited landslide inventory data. Landslides 9:357–369
ESRI (2011) ArcGIS Desktop: Release 10. Environmental Systems Research Institute, Redlands, CA
Foster MA, Kelsey HM (2012) Knickpoint and knickzone formation and propagation, South Fork Eel River, northern California. Geosphere 8:403–416
Gallen SF, Wegmann KW, Frankel KL, Hughes S, Lewis RQ, Lyons N, Paris P, Ross K, Bauer JB, Witt AC (2011) Hillslope response to knickpoint migration in the Southern Appalachians: implications for the evolution of post–orogenic landscapes. Earth Surf Process Landforms 36:1254–1267
Gallen SF, Wegmann KW, Bohnenstiehl DR (2013) Miocene rejuvenation of topographic relief in the southern Appalachians. GSA Today 23:4–11
Gardner TW (1983) Experimental study of knickpoint and longitudinal profile evolution in cohesive, homogenous material. Geol Soc Am Bull 94:664–672
GRASS Development Team (2011) Geographic Resources Analysis Support System (GRASS) Software, Version 6.4.1. Open Source Geospatial Foundation. http://grass.osgeo.org.
Hack JT (1975) Dynamic equilibrium and landscape evolution. In: Melhorn WL, Flemal RC (eds) Theories of landform development. State University of New York Press, New York, pp 87–102
Hadley JB, Goldsmith R (1963) Geology of the eastern Great Smoky Mountains, North Carolina and Tennessee. US Geological Survey Professional Paper 349B:1–118
Haralick RM, Shanmugam K, Dinstein I (1973) Textural features for image classification. IEEE Transactions on Systems, Man, and Cybernetics 3:610–621
Hatcher RD (1978) Tectonics of the western Piedmont and Blue Ridge, southern Appalachians: review and speculation. Am J Sci 278:276–304
Hershfield DM (1961) Rainfall frequency atlas of the United States for durations from 30 minutes to 24 hours and return periods from 1 to 100 years. U.S. Department of Commerence Weather Bureau Technical Paper 40.
Hovius N, Stark C, Tutton M, Abbott L (1998) Landslide-driven drainage network evolution in a pre-steady-state mountain belt: Finisterre Mountains, Papua New Guinea. Geology 26:1071–1074
Howard A (1994) A detachment-limited model of drainage-basin evolution. Water Resour Res 30:2261–2285
Ijjasz-Vasquez EJ, Bras RL (1995) Scaling regimes of local slope versus contributing area in digital elevation models. Geomorphology 12:299–311
Jungers MC, Bierman PR, Matmon A, Nichols K, Larsen J, Finkel R (2009) Tracing hillslope sediment production and transport with in situ and meteoric 10Be. J Geophys Res 114:1–16
Kochel RC (1990) Humid fans of the Appalachian Mountains. In: Rachocki AH, Church M (eds) Alluvial fans: a field approach. John Wiley & Sons, New York, pp 109–129
Korup O, Densmore AL, Schlunegger F (2010) The role of landslides in mountain range evolution. Geomorphology 120:77–90
Leigh DS, Webb PA (2006) Holocene erosion, sedimentation, and stratigraphy at Raven Fork, southern Blue Ridge Mountains, USA. Geomorphology 78:161–177
Madden M, Jackson P, Seavey R, Seavey J (2004) Digital vegetation maps for the Great Smoky Mountains National Park final report. Center for Remote Sensing and Mapping Science, Department of Geography, University of Georgia.
Malamud BD, Turcotte DL, Guzzetti F, Reichenbach P (2004) Landslide inventories and their statistical properties. Earth Surf Process Landforms 29:687–711
MATLAB (2009) MATLAB version 7.8.0. The MathWorks Inc., Natick, Massachusetts.
Matmon A, Bierman P, Larsen J, Southworth S, Pavich M, Finkel R, Caffee M (2003) Erosion of an ancient mountain range, the Great Smoky Mountains, North Carolina and Tennessee. Am J Sci 303:817–855
Martha TR, Kerle N, Jetten V, Van Westen CJ, Kumar KV (2010) Characterizing spectral, spatial, and morphometric properties of landslides for semi-automatic detection using object-oriented methods. Geomorphology 116:24–36
McCauley J, Engel B (1995) Comparison of scene segmentations: SMAP, ECHO, and maximum likelihood. IEEE Trans Geosci Remote Sensing 33:1313–1316
Mitasova H, Hofierka J (1993) Interpolation by regularized spline with tension: II. Application to terrain modeling and surface geometry analysis. Mathematical Geology 25:657–669
Mitasova H, Mitas L (1993) Interpolation by regularized spline with tension: I theory and implementation. Math Geol 25:641–655
Moine M, Puissant A, Malet J-P (2009) Detection of landslides from aerial and satellite images with a semi-automatic method. Application to the Barcelonnette basin (Alpes-de-Haute-Provence, France). In: Malet JP, Remaitre A, Bogaard T (eds) Landslide processes: from geomorphic mapping to dynamic modeling. CERG, Strasborg, France, pp 63–68
Montgomery D, Foufoula-Georgiou E (1993) Channel network source representation for Digital Elevation Models. Water Resour Res 29:3925–3934
Neary DG, Swift LW (1987) Rainfall thresholds for triggering a debris avalanching event in the southern Appalachian Mountains. Rev Eng Geol 7:81–92
Neuhäuser B, Damm B, Terhorst B (2012) GIS-based assessment of landslide susceptibility on the base of the Weights-of-Evidence model. Landslides 9:511–528
North Carolina Flood Mapping Project (2011) Floodplain mapping information system lidar data, North Carolina Flood Mapping Project. http://floodmaps.nc.gov. Accessed 12 December 2011.
Nichol J, Wong MS (2005) Satellite remote sensing for detailed landslide inventories using change detection and image fusion. Int J Remote Sens 26:1913–1926
Pack RT, Tarboton DG, Goodwin CN (1998) The SINMAP approach to terrain stability mapping. 8th Congress of the International Association of Engineering Geology, Vancouver, British Columbia, Canada 21–25 September 1998
Pazzaglia FJ, Gardner TW, Merritts DJ (1998) Bedrock fluvial incision and longitudinal profile development over geologic time scales determined by fluvial terraces. Geophysical Monograph-American Geophysical Union 107:207–236
Quinn P, Beven K, Chevallier P, Planchon O (1991) The prediction of hillslope flow paths for distributed hydrological modelling using digital terrain models. Hydrol Process 5:59–79
Rivenbark BL, Jackson CR (2004) Average discharge, perennial flow initiation, and channel initiation: Small southern Appalachian basins. Journal of the American Water Resources Association 40:639–646
Seidl M, Dietrich W (1992) The problem of channel erosion into bedrock. Catena Supplement 23:101–101
Southworth S, Schultz A, Denenny D, Triplett J (2005) Surficial geologic map of the Great Smoky Mountains National Park Region, Tennessee and North Carolina. US Geological Survey Professional Report and Geological Map, scale 1:100,000.
Stock JD, Dietrich WE (2003) Valley incision by debris flows: evidence of a topographic signature. Water Resour Res 39:1089
Stock JD, Montgomery DR (1999) Geologic constraints on bedrock river incision using the stream power law. J Geophys Res 104:4983–4993
Strahler AN (1952) Hypsometric (area-altitude) analysis of erosional topography. Geological Society American Bulletin 63:1117–1142
Tarboton DG (1990) The analysis of river basins and channel networks using digital terrain data. Bras RL (Ed), Massachusetts Institute of Technology thesis: http://hdl.handle.net/1721.1/39956.
Tarolli P, Dalla Fontana G (2009) Hillslope-to-valley transition morphology: new opportunities from high resolution DTMs. Geomorphology 113:47–56
Tucker G, Slingerland R (1997) Drainage basin responses to climate change. Water Resour Res 33:2031–2047
Van Den Eeckhaut M, Poesen J, Verstraeten G, Vanacker V, Nyssen J, Moeyersons J, van Beek LPH, Vandekerckhove L (2007) Use of LIDAR-derived images for mapping old landslides under forest. Earth Surf Process Landforms 32:754–769
Wegmann KW (2006) Digital landslide inventory for the Cowlitz County urban corridor, Washington; version 1.0: Washington Division of Geology and Earth Resource Report of Investigations 35, 24 pp., 14 maps, scale 1:24,000.
Whipple KX, Tucker GE (1999) Dynamics of the stream-power river incision model: implications for height limits of mountain ranges, landscape response timescales, and research needs. J Geophys Res 104:17,661–17,674
Witt AC (2005) A brief history of debris flow occurrence in the French Broad River Watershed, western North Carolina. NC Geogr 13:58–82
Wobus CW, Whipple KX, Kirby E, Snyder NP, Johnson J, Spyropolou K, Crosby BT, Sheehan D (2006) Tectonics from topography: procedures, promise, and pitfalls. In: Willett SD, Hovius N, Brandon MT, Fisher DM (eds) Tectonics, climate and landscape evolution: geological society of america special paper 398, Penrose Conference Series., pp 55–57
Woodruff JF (1971) Debris avalanches as an erosional agent in the Appalachian Mountains. J Geogr 70:399–406
Wooten R, Gillon KA, Witt AC, Latham RS, Douglas TJ, Bauer JB, Fuemmeler SJ, Lee LG (2008) Geologic, geomorphic, and meteorological aspects of debris flows triggered by Hurricanes Frances and Ivan during September 2004 in the Southern Appalachian Mountains of Macon County, North Carolina (Southeastern USA). Landslides 5:31–44

N. J. Lyons (✉) · H. Mitasova · K. W. Wegmann
Department of Marine, Earth, and Atmospheric Sciences,
North Carolina State University,
2800 Faucette Drive, Raleigh, NC 27695, USA
e-mail: njlyons@ncsu.edu